ADVANCED THERAPEUTICS
www.advtherap.com

Airplug-Mediated Isolation and Centralization of Single T Cells in Rectangular Microwells for Biosensing

*Pavithra Sukumar, Muhammedin Deliorman, Ayoola T. Brimmo, Roaa Alnemari, Deena Elsori, Weiqiang Chen, and Mohammad A. Qasaimeh**

Sorting cells in a single cell per microwell format is of great interest to basic biological studies, biotherapeutics, and biosensing including cell phenotyping. For instance, isolation of individual immune T cells in rectangular microwells has been shown to empower the multiplex cytokine profiling at the single cell level for therapeutic applications. The present study, shows that there is an existing bias in temporal cytokine sensing that originates from random "unpredicted" positions of loaded cells within the rectangular microwells. To eliminate this bias, the isolated cells need to be well-aligned with each other and relative to the sensing elements. Hence, an approach that utilizes the in situ formation and release of airplugs to localize cells toward the center of the rectangular microwells is reported. The chip includes 2250 microwells (each 500 × 50 × 20 μm^3) arranged in nine rows. Results show 20% efficiency in trapping single T cells per microwells, where cells are localized within ± 3% of the center of microwells. The developed platform could provide real-time dynamic and unbiased multiplex cytokine detection from single T cells for phenotyping and biotherapeutics studies.

1. Introduction

Immune T cells are among most vibrant and specialized cells in our bodies that possess unique responses to disease conditions. They are also very distinctive in their ability to respond against infections including human immunodeficiency virus [1] and Ebola virus.[2] For instance, they dynamically secrete several types of cytokines as part of the defense mechanisms.[3,4] However, the immune status of the patients changes with the disease progression, thus making effective immunomodulatory therapies very challenging in clinical practices.[3] Therefore, quantitative and real-time analysis of the cytokine profiles of individual T cells is needed for precise determination and characterization of the "immunophenotype" of patients for personalized medication.[4] Such cytokine profiling, on the other hand, requires effective isolation of single T cells from a heterogeneous mixture of multiple cell subsets so that the individual contributions of specific subpopulations within large networked communities would be determined.[4]

To date, several methods, such as serial dilution,[5] random cell seeding,[6] and fluorescence-activated cell sorting,[7] have been developed to sort T cells based on their characteristic surface markers. However, these methods can only show "average" phenotypes for large population of T cells because of their limited ability to achieve single cell resolution. Studying T cells at single cell levels, on the other hand, provides a great deal of information in the areas of genomics,[8] proteomics,[9] cell–cell interactions,[10] and therapeutics[11] for detailed identification and characterization of cells' heterogeneity and accurate decoupling of cell–stimulus interactions.

Microfluidics offer a wide range of miniaturized devices that can be highly sensitive toward the multiplex analysis of cellular functions at single cell resolution, typically because of the controllability of small volumes of reagents and ability to run multiple/parallel measurements in real time.[12] Several of the microfluidic-based technologies utilize external fields such as electric,[13] acoustic,[14] magnetic,[15] and gradient[16] to isolate single T cells. Alternatively, passive technologies uses hydrodynamics and gravity[17] to "entrap" cells in various microstructures, such as microwells,[18,19] guiding structures,[20] and microtraps.[21] Massive microwell arrays are favorable because of their simplicity and scalability, which makes them attractive especially when integrated with biosensing platforms such as arrays of tagged antibody barcodes.[22] After isolation, the biosensing platforms are typically placed on the top of isolated cells to measure cytokines by fluorescent read-outs.[23–25] While circular and square

P. Sukumar, Dr. M. Deliorman, A. T. Brimmo, R. Alnemari, Prof. M. A. Qasaimeh
Division of Engineering
New York University Abu Dhabi (NYUAD)
P.O. Box 129188, Abu Dhabi, UAE
E-mail: mohammad.qasaimeh@nyu.edu
Prof. D. Elsori
Department of Applied Sciences and Mathematics
Abu Dhabi University
P.O. Box 59911, Abu Dhabi, UAE
Prof. W. Chen
Department of Biomedical Engineering
New York University
Brooklyn, NY 11201, USA
A. T. Brimmo, Prof. W. Chen, Prof. M. A. Qasaimeh
Department of Mechanical and Aerospace Engineering
New York University
Brooklyn, NY 11201, USA

The ORCID identification number(s) for the author(s) of this article can be found under https://doi.org/10.1002/adtp.201900085

DOI: 10.1002/adtp.201900085

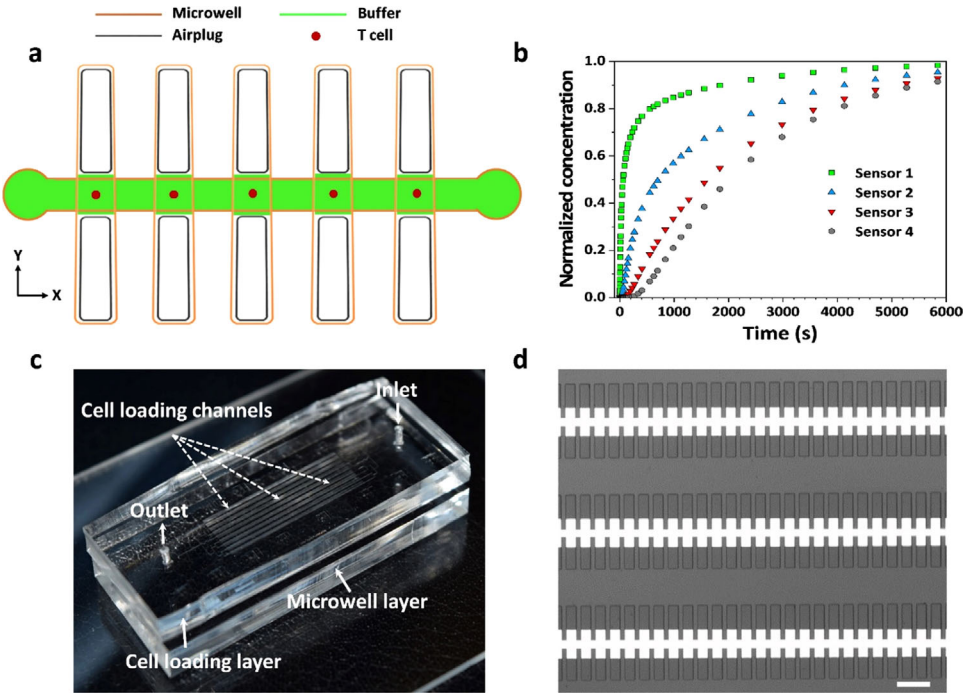

Figure 1. Airplug-mediated isolation and centralization of single T cells in rectangular microwells. a) Schematic representing the device concept. b) Numerical simulation of the detection of interleukin-6 (IL-6) released from a single T cell when sensors are placed 100 µm apart from each other. c) Photograph of the PDMS microfluidic device featuring the cell loading (top) and microwell (bottom) layers, both thermally (physically) bonded to each other. Each of the cell loading channels (9 total) are 45 mm long and 20 µm wide, whereas each of the microwells (2250 total) are 500 µm long, 50 µm wide, and 20 µm deep. d) Micrograph shows the airplugs formed on both sides of the microwells along the cell loading channels of the microfluidic device, where bright colors indicate the regions of the wells occupied with liquid. Scale bar is 200 µm.

microwells have shown to be efficient,[26,27] rectangular microwells offer multiplexed cytokine profiling.[22]

A series of interesting studies[21–23] suggested direct loading of T cells onto an array of rectangular microwells as an efficient method to isolate single immune cells. However, due to variations in controllability of pipetting and serial dilutions, the isolation efficiency (<10%) resulted in a low number of single T cells per microwells. The method also showed large differences (>200 µm) in the relative positions of cells within the rectangular microwells. In acute viral infections, however, the variations in the cell positions relative to sensing assays (e.g., antibody barcodes) could result in biased profiling of cytokines elicited by individual T cells.[28] Thus, for precise cell immunophenotyping that is required for personalized medicine,[26] and in particular, for specific (unbiased) profiling of the cytokine releases from each immune cell,[29] there is still a need for an approach that isolates high number of single T cells per rectangular microwells and centralizes them relative to each other.

In the present work, we first show by numerical simulation that when isolated single T cells are decentralized in the rectangular microwells, the real-time cytokine sensing is biased (Figure S1a, Supporting Information). To minimize this bias, we then present an airplug-mediated combined approach for isolation and centralization of single T cells in rectangular microwells of a polydimethylsiloxane (PDMS)-based microfluidic device (**Figure 1**a). The device consists of two layers, one having an array of rectangular microwells and the other cell loading channels, both assembled via thermal reversible bonding. Within the microwells, the isolation and centralization of single T cells are carried out by combining temporarily formed airplugs and antibody-coated microwell surfaces, where airplugs are to align cells through induced pressure and antibodies are to selectively capture cells through antibody–antigen interactions. This way, upon the release of airplugs, we show that the device can be disassembled with minimal dislocations of isolated cells. Additionally, using the device we show preliminary data on the cytokine detection via antibody–antigen binding. Overall, the presented approach offers efficient isolation and precise centralization of a large amount of single T cells within rectangular microwells that is expected to provide real-time dynamic cytokine profiling for accurate therapeutics.

2. Results

2.1. Bias in Sensing Due to Relative Location of Cells within Microwells

Due to low concentrations of cytokines released by single T cells,[27] real-time dynamic cytokine sensing in the microwells can be biased when the locations of cells differ relative to the multiple fixed sensors[28] (Figure S1a-i,ii, Supporting Information). To evaluate the possibilities, we first developed a numerical model where a single T cell with a 10 µm diameter was located in a 350 µm long rectangular microwell and four sensors, positioned 100 µm apart from each other, were placed at the top

of the microwell in a way that the cell resides under one of the sensors (Figure S1a-i, Supporting Information). Here, the rectangular microwell (20 μm height) was used as model due to its geometrical favorability to accommodate multiplex cell analysis using tagged antibody barcodes. In addition, the number and dimensions of the sensors were chosen to represent an example for an easy fabrication of the sensor platform. For example, in cases when longer microwells are desired, 10, 15, or 20 sensors can be used in a similar way. Ideally, smaller microwells with higher number of "closely" positioned biosensing stripes can provide minimal bias in sensing, however their manufacturing would require complicated microfabrication processes. Nevertheless, in our work we obtained the transient numerical solutions for the scenario where interleukin-6 (IL-6)[30] proteins are continuously released from the cell isolated in a rectangular microwell (Figure 1b). As expected, the IL-6 concentrations detected by all the sensors raised exponentially relative to concentration value of 1. However, while the concentration readings from the sensor placed 10 μm away from the cell began to saturate in about 2 min, the readings from the other sensors placed 100, 200, and 300 μm away from the cell began to saturate in 40, 60, and 69 min, respectively (Figure S1a-iii, Supporting Information). These findings suggested that, in the proposed scenario, a 100 μm misalignment of the isolated cell within an array of rectangular microwells could increase the cytokine sensing time from 2 to 40 min. In a scenario when cell resides 50 μm away from one of the sensors (Figure S1a-ii, Supporting Information), the concentration readings from the sensor will peak in about 1 min, followed by saturation of the reading at 40 min. The readings of the sensors placed 150, 250, and 350 μm away from the cell began to saturate in about 50 min (Figure S1a-iv, Supporting Information).

The exact nature of cytokine release from single cells is not yet fully understood, but few indications pointed at the possibility of their intermittent release.[26] To evaluate the extent of bias in this type of release, we additionally calculated IL-6 temporal concentrations at 10 s release intervals (Figure S1c-i–iv, Supporting Information). Interestingly, the reduced IL-6 peak concentration relative to sensors' distance from the cell suggested that the bias in the IL-6 measurements increases as cells' misalignment increases.

2.2. Device Layout and Assembly

In designing the microfluidic device, the key issue was to assist the isolation and centralization of the T cells in rectangular microwells so that, for instance, the integration of stripes of tagged antibody barcodes would be feasible for more precise cell immunophenotyping and specific (unbiased) cytokine profiling in real time. To address this issue, we designed a two-layer microfluidic device (Figure 1c), where both layers were made out of PDMS. The top layer consisted of nine cell loading channels, each with dimensions of 50 μm × 20 μm (width × height), and the bottom layer consisted of 250 × 9 arrays of microwells (total of 2250), each with dimensions of 500 μm × 50 μm × 20 μm (length × width × height) that can hold up to 0.5 nL liquid.

Following aligning the cell loading and the microwell layers, which provided ≈50 μm × 50 μm square areas in the middle of the microwells, the layers were allowed to thermally (reversibly) seal in air and placed in an oven at 60 °C to further improve the sealing and the hydrophobicity of the PDMS.[31] Among tested conditions for reversible bonding (e.g., 5, 10, and 15 h of heating), 15 h tended to form strong bondage between the PDMS layers without any leakage issues even when flow rates of up to 1000 μL h^{-1} were used.

2.3. Airplug Formation and Characterization

To minimize the relative positions of isolated cells within the microwells, prior to each cell loading experiments airplugs were formed and used as mediators in the isolation and centralization of the single T cells. For this, PBS was first passed through the channels, where both the small dimensions of the microwells and the highly hydrophobic nature of thermally bonded PDMS layers have led to formation of airplugs in each side of the microwells of the microfluidic device (Figure 1d). This way, 4500 discrete airplug chambers were formed (2250 in each side of the microwells). Overall, airplugs were shorter near the channels' inlet and their length increased toward the channels' outlet due to pressure drop in the loading channels when passing PBS. As illustrated schematically in **Figure 2**a, this resulted in gradual decrease in liquid occupancy starting from the channels' inlet. Therefore, for analysis purposes, we subdivided the regions of interest within the microfluidic channels into three sections (upstream, midstream, and downstream) based on the length of liquid occupancy within the microwells along the channels. Each section consisted of about 80 microwells per row (Figure 2a).

Following passing the PBS at different flow rates, the formation of airplugs was recorded in time-lapse movies and the change in the length of liquid occupancy per microwells was measured for 15 microwells in each section. Among the tested flow rates (Figure 2b), 500 μL h^{-1} resulted in shorter liquid occupancy (i.e., longer airplug lengths) with minimal volume change (from ≈0.12 to 0.08 nL, inlet to outlet) within the microwells. Additionally, at 500 μL h^{-1} flow rate the total amount of time (≈25 s) needed to form the desired airplugs in the microwells was least among all other tested flow rates (Figure 2c).

2.4. Airplug Release

Our follow-up requirement in optimizing the device was to minimize the displacement of isolated and centralized single T cells after releasing the airplugs. Such cell displacements could especially result from the pressure changes within the microwells during the airplug retractions. Hence, to characterize the airplug release dynamics, we initially passed fluorescein (green) dyes at 500 μL h^{-1} flow rates to generate the airplugs within the microwells (Figure S2a, Supporting Information). This way, it was easy to visually distinguish the regions within the wells that were filled with liquid from the airplugs. Then, rhodamine dyes (red) were flushed at varying flow rates (from 100 to 750 μL h^{-1}) to release the airplugs. Interestingly, experiments revealed that the airplug release was much faster with increased flow rates

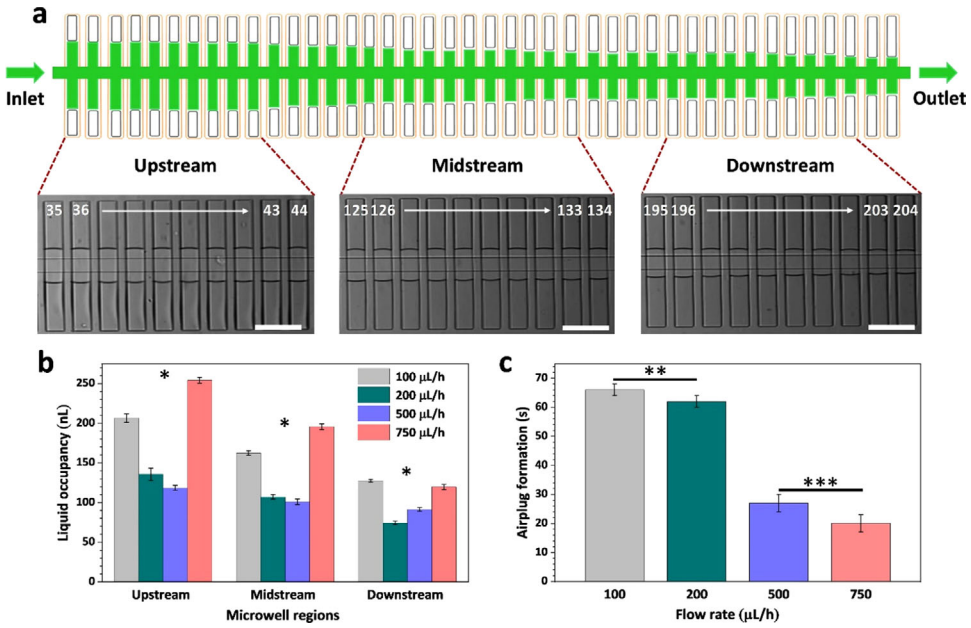

Figure 2. Characterization of airplug formation. a) Schematic, along with representative optical images, reveals the upstream, midstream, and downstream sections of the microwell rows along one of the device's cell loading channel. The gradual decrease in the liquid occupancy (green) starting from channel inlet is due to pressure drop within the channel. In the microscopy images, channel numbers are given to represent the positions of the upstream, midstream, and downstream sections relative to each other and within the channel. Scale bars are 125 µm. b,c) Characterization of the airplugs in the upstream, midstream, and downstream sections suggested that 500 µL h^{-1} flow rate was optimal in terms of minimal change in the liquid occupancy (from ≈0.12 to 0.08 nL, inlet to outlet) within the microwells across the channel and the total amount of time (≈25 s) needed to form the desired airplugs. Values and error bars represent Mean ± SD. from triplicate measurements ($n = 3$). *, **, and *** are statistically significant at $p < 0.05$ using t-test.

(Figure S2b, Supporting Information), most likely due to steeper pressure drops within the microwells lengths. Moreover, results showed that after 1 min of rhodamine flushing, airplugs were slowly compressed toward the ends of the microwells and eventually released. During their release, the change in the length of the airplugs with time varied depending on the position of airplugs within the loading channel. As such, the ones formed in the upstream sections resulted in faster release (after 12 min), followed by the ones in the midstream (after 25 min), and downstream (after 40 min) sections (Figure S2c, Supporting Information).

2.5. Single T Cell Isolation in Rectangular Microwells

The airplug-mediated single cell isolation efficiency of the developed device was evaluated using human lymphocyte T (Jurkat) cells. In the efficiency evaluation, T cells were fluorescently labeled and passed at 10^6 cells mL^{-1} concentrations using varying flow rates. As a result, the number of cells isolated in each of the microwells (**Figure 3**a) were counted and recorded. Following, the overall single cell isolation efficiency (i.e., cell occupancy) per microwells was calculated using $\frac{N_s}{N_t} \times 100$, where N_s is the number of single isolated cells per microwells and N_t is the total number of microwells.

When T cells were introduced at low flow rates (≤50 µL h^{-1}), very few cells were isolated in the microwells. Similarly, increasing the flow rates to 100 µL h^{-1} did not significantly change the single cell isolation efficiency. Therefore, in order to improve efficiency, we introduced a pulsatile flow regime in which cells were allowed to sediment in microwells for extended times. In this context, we performed experiments at 1-, 5-, and 10-min stationary flows for cells to sediment in a total of five loading pulses. Results using 100 µL h^{-1} flow rate showed that at 1-min sedimentation times cells were washed off in the subsequent pulsatile flows, most likely because there was not enough time for them to reach the bottom of the microwells (Figure S3a, Supporting Information). At 10-min sedimentation times, on the other hand, cells were sedimented as aggregates, resulting for >2 cells to make it to the same microwell (Figure S3a, Supporting Information). Hence, these sedimentation times limited the single T cell occupancy per microwells. At 5-min sedimentation times, on the other hand, cells were isolated with high efficiency, which resulted in 20% of the microwells to be occupied with single T cells (Figure 3b,c). In comparison, combining 50 and 200 µL h^{-1} flow rates with 5-min sedimentation times resulted in low percentage (≈1% and 2%, respectively) of microwells to be occupied with single T cells (Figure 3c).

Additional optimization experiments were carried out by passing cells at 50, 100, and 200 µL h^{-1} flow rates (Figure S3b, Supporting Information) over the channels with and without airplugs. Interestingly, the airplug-mediated single cell isolation efficiency was ≈6 times higher than the one achieved without airplugs (19.7% and 3.4%, respectively, Figure 3d), mainly due to the pressure oscillations[32] induced by the entrapped airplugs. As such, passing cells over the airplug-enabled channels results in oscillations of the airplugs, which creates pressure differences at the air–liquid interface of the microwells. The pressure

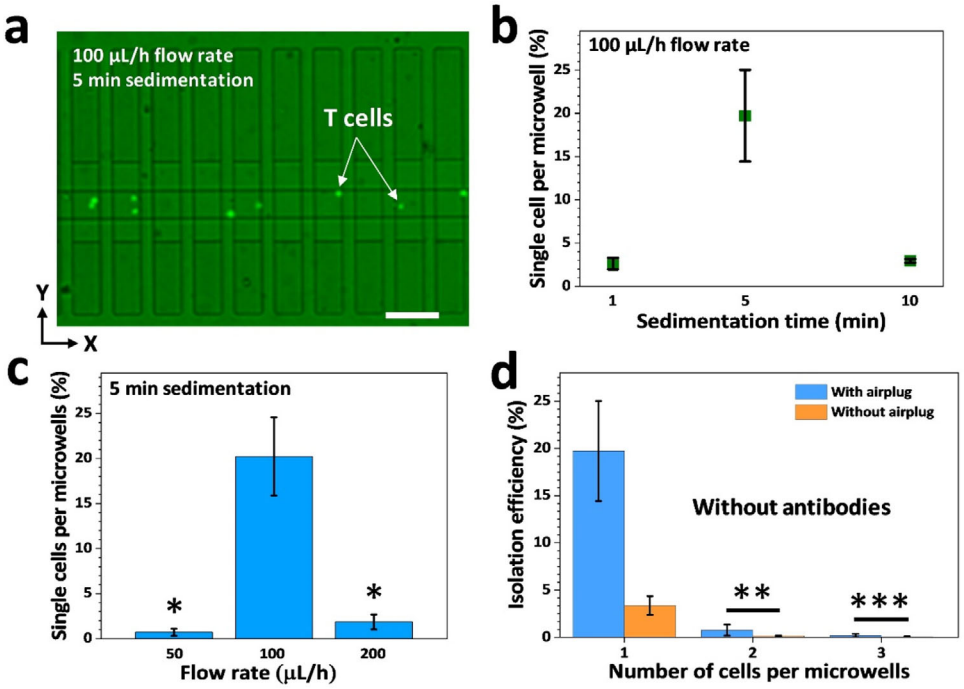

Figure 3. Characterization of airplug-mediated single cell isolation. a) Fluorescence image shows isolated single T cells (green) confined by in situ generated airplugs in microwells. Scale bar is 100 µm. b,c) The characterization of single T cell isolation at varying sedimentation times and pulsatile flow rates suggested that passing cells at 100 µL h^{-1} flow rate and allowing them to sediment for 5 min in a total of five pulsations results in 20% of the microwells to be occupied with single cells. At 50 µL h^{-1} and 200 flow rates, the percentage of microwells occupied with single cells dropped to ≈1% and 2%, respectively. d) Compared to without airplugs (control), airplug-mediated single T cell isolation offered ≈six times better isolation efficiency. Values and error bars represent Mean ± SEM. from triplicate measurements ($n = 3$). *, **, and *** are statistically significant at $p < 0.05$ using t-test.

difference then helps the passing cells to "slow down" within the microwells.[33] At flow rates > 200 µL h^{-1}, the oscillations, and consequently the fluid microvortices, are amplified. Therefore, the time that takes to release the airplugs is shorter. This results in cells getting displaced or even escaped from the microwells easily. At flow rates ≤ 200 µL h^{-1}, the microvortices are less influential and the time that takes to release the airplugs is longer. This results in minimal displacement of the cells within the microwells. Finally, despite of the pressure differences between the upstream, midstream, and downstream sections, it was observed that single cells were isolated in >70% of the microwells in the upstream and midstream sections with 86.5% and 60% efficiencies, respectively, while two to three cells per microwells—although in a lesser (<30%) extent—were isolated in the downstream sections with 27.5% efficiency (Figure S3c, Supporting Information). Additionally, the overall displacement of the cells within these regions remained the same upon the release of the airplugs. The airplug expansion, on the other hand, was minimal during the sedimentation of the cells, which favored their centralization within the microwells.

2.6. Centralization of T Cells

To minimize the displacements of isolated cells after the release of the airplugs and subsequent peel off the cell loading layer from the microwell layer (**Figure 4**a), our next step was toward immobilizing the isolated single T cells through antibody–antigen capture. Here, the antibody capture mechanism is also a needed step when selective isolation of T cells from highly heterogeneous mixtures of other cells in blood is desired. Therefore, following the formation of the airplugs, we have further introduced chemical modification steps[34] to the microwell surfaces for the immobilization of anti-$CD3^+$ antibodies (commonly used in the evaluation of $CD3^+$ expressions in T cells)[35,36] via covalent bondages. This way, T cells could be selectively and firmly attached in between the airplugs of the rectangular microwells. During the functionalizion steps of the device, the changes in the lengths of the airplugs were minimal when 20 µL h^{-1} flow rate was used to pass the solutions (Figure S4-a–c, Supporting Information). As a result, isolated single T cells remained captured and centralized within the rectangular microwells when airplugs were released during flushing channels with PBS at 200 µL h^{-1} flow rates (Figure S4d, Supporting Information).

Overall, our results showed that without antibodies, isolated single T cells tended to randomly displace their positions upon the release of the airplugs (Figure 4b). However, having the antibodies confirmed the firm attachment of the cells in the central regions of the microwells (Figure 4c). Additional experiments showed that airplug-mediated isolation resulted in cells to be localized within ±30 µm of the microwells' central lines, while control experiments without airplugs resulted in ±150 µm cell localizations. Nonetheless, after the release of the airplugs, cells experienced ±120 µm overall displacement relative to their initial positions (Figure 4d). On the contrary, when the microwells

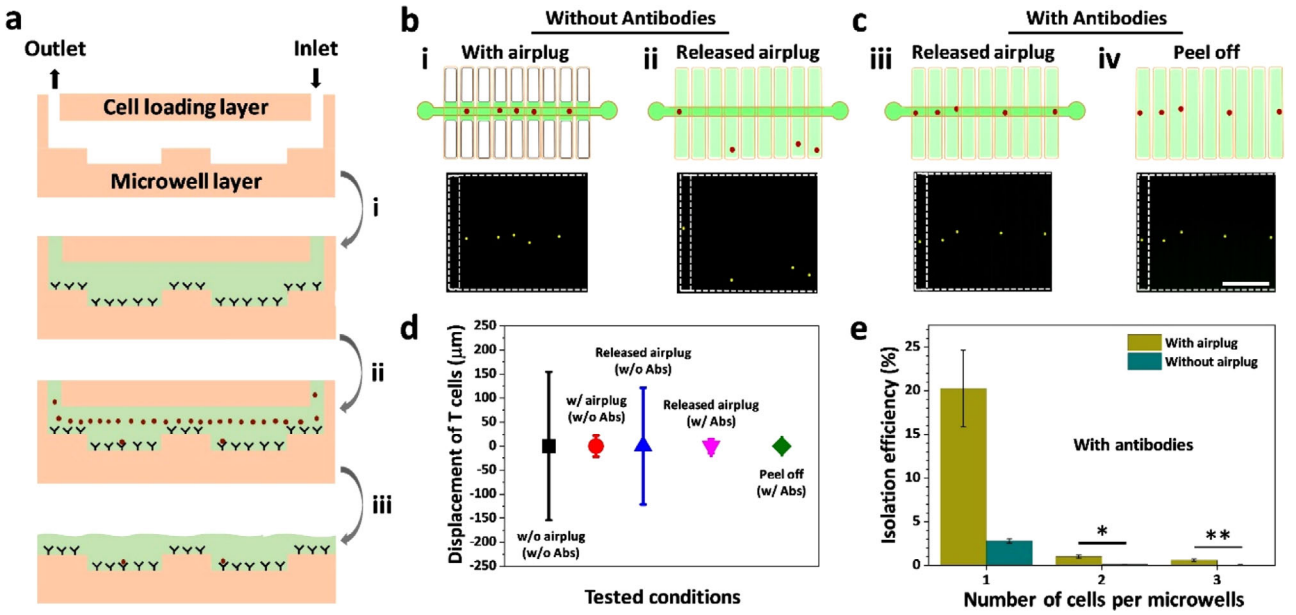

Figure 4. Centralization of cells through antibody capture. a) Conceptual schematic of the microfluidic device showing i) antibody functionalization (black Y shapes), ii) cell loading and capture (red dots), and iii) layer separation (i.e., peel off) as an application for immunophenotyping of centralized cells. b,c) Illustrative schematics and representative fluorescence images show that without antibodies, isolated cells displace (decentralize) after the release of airplugs (i,ii). Whereas with antibodies, the displacement of cells is minimal upon release of airplugs and peel off the cell loading layer (iii,iv). Scale bars are 200 μm. d) The dependence of displacement of isolated cells ($n = 76$) within the microwells on various tested conditions reveals that antibody-captured centralized cells show minimal displacement both after the release of airplugs (+19 μm and −22 μm) and peel off the cell loading layer (+22 μm and −22 μm). Data sets in tested conditions are statistically significant at $p < 0.05$ using t-test. e) Compared to without airplugs (control), the isolation efficiency of airplug-mediated single cell capture in antibody-coated microwells was similar (20.1%) to the isolation efficiency of single cell isolation in microwells without antibodies, as shown in Figure 3d. Values and error bars represent Mean ± SEM. from triplicate measurements ($n = 3$). *, **, and *** are statistically significant at $p < 0.05$ using t-test.

were coated with anti-CD3$^+$ antibodies, the firmly attached single T cells showed minimal (less then ±15 μm) relative displacements, both after the release of the airplugs and the peeling off the cell loading layer from the microwell layer (Figure 4c,d). This finding further confirmed that antibodies are needed for the firm centralization of the T cells as equivalently needed for selective isolation. Finally, single T cell occupancy per microwells showed similar trend on anti-CD3$^+$ coated microwells as when cells were solely isolated without antibodies (Figure 4e). As such, when localized by antibodies, the single cell isolation efficiency per microwells with airplugs was 20%, whereas it was only 3% when they were localized without airplugs.

2.7. Cytokine Analysis

To investigate the applicability of the developed device in cytokine detection from single T cells, preliminary experiments were conducted to measure the release of IL-2 via antibody–antigen binding (**Figure 5**). As concept, phorbol myristate acetate (PMA) and ionomycin were used to stimulate the T cells for 60, 120, and 240 min and anti-IL-2 antibody coated stripes (2 for each microwell with an uncoated region in between them, all 100 μm in width) were used to detect the IL-2 secretion following each activation. As expected, the analysis of spot sizes in fluorescence images revealed that the increase in IL-2 secretion is time dependent. Results also showed differences in the spot intensities of released IL-2, which we attributed to the heterogeneity among the stimulated single cells. The bias in sensing due to position of cells relative to sensing stripes was also achieved, although the high noise-to-signal ratio in the background of fluorescence images and the possible saturation of the sensing antibodies (Figure S5, Supporting Information). Future studies will involve optimizing the imaging parameters and quantifying the antibody saturation with respect to the amount of cytokine release.

Importantly, the antibody–antigen interaction—used in the centralization of the T cells—may alter the cell behavior, knowingly that such interaction requires the activation of Toll-like receptors in the cell capture process.[37] This, in turn, could stimulate the expression of various proteins and thus jeopardize the true reflection of the immunophenotypes in vivo. Yet, to activate the T cells for immune response, stimulants such as PMA and ionomycin are still needed to act directly on inositol 1,4,5-triphosphate (IP3) and protein kinase C (PKC) pathways so that more proteins could be expressed.[38] Nevertheless, more detailed experiments are left for future studies to investigate the contribution of capture antibodies to the total immune response of T cells.

3. Discussion

This work presents a new approach to efficiently isolate and centralize single T cells in rectangular microwells by using in situ formed airplugs and selective capture antibodies. Considering

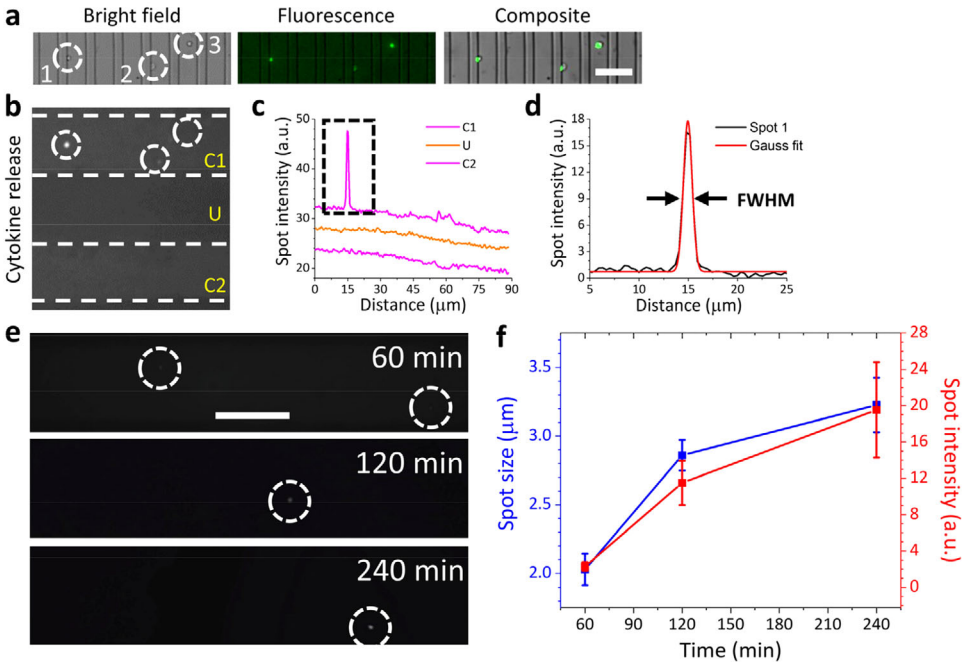

Figure 5. Cytokine detection and analysis. a) Representative bright field images of T cells (white-dashed circles) trapped within the microwells of the developed device. After 60 min of cytokine release, staining cells with calcein AM (green fluorescence) confirmed that the cells remained alive within the microwells. The composite image is also shown for comparison. Scale bar is 100 μm. b) Following stimulation of cells 1, 2, and 3 with PMA and ionomycin, anti-IL-2 antibody sensing stripes, C1 and C2, with an uncoated (U) region in between them, were immediately positioned on the top of the cells within the microwells for the detection of the cytokine release. c) The intensity analysis across C1, U, and C2 regions was used to reveal the presence of the cytokine spots (e.g., black-dashed rectangle) with respect to their positions on the antibody sensing stripes. d) Fitting the spots to Gauss probability density function further allowed to quantify the spot sizes (as full width at half maximum, FWHM) and the maximum spot intensities. e) Representative fluorescence images showing the cytokine release intensity from single T cells after 60, 120, and 240 min of stimulation. Scale bar is 200 μm. f) Quantification of spot sizes and intensities in fluorescence images reveals that the increase in IL-2 secretion is time dependent. Values and error bars represent Mean ± SEM. from triplicate measurements ($n = 3$).

the importance of the dynamic and unbiased sensing in real time, the approach could allow for quick and precise profiling of the cytokine release from individual T cells. As such, smaller in size microwells and denser in number biosensing stripes can potentially reduce the bias in sensing, although their microfabrication could be time-consuming and costly. Regardless, our overall motive is to combine the developed approach with the existing sensing techniques such as enzyme-linked immunosorbent assay (ELISA)-based barcode sensing[22] and label-free localized surface plasmonic resonance[39] for precise immunophenotypic characterization of isolated single immune cells. Utilizing rectangular microwells is required for multiplex biosensing where a different antibody barcodes (e.g., anti-IL-6, antitumor necrosis factor, anti-interferon gamma, etc.) can be orthogonally placed atop in a mosaic configuration.

As revealed by our numerical calculations, depending on the transient cytokine release mechanisms, misalignment of the cells within the microwells relative to the sensors brings a bias to the detection time—and consequently, the accuracy—of the released cytokine concentrations. Therefore, the critical steps involved in designing the device include in situ formation of airplugs for centralized cell loading, functionalization of the microwells with antibodies for selective cell isolation and firm capture, and thermal (physical) bondage of the cell loading layer to the microwell layer for the subsequent replacement of the cell loading layer with multiplexed biosensing platforms such as arrays of tagged antibody barcodes.

In a recent study,[22] Lu and coworkers demonstrated the use of a tagged antibody barcodes to simultaneously detect 14 cytokines from a large (>1000) population of T cells isolated in rectangular microwells. Remarkably, in this way they were able to correlate cell heterogeneity with cytokines release. To isolate the cells, they pipetted a suspension of cells onto the microwells and allowed them to sediment by gravity, which resulted in 10% single cell per microwell isolation efficiency. Additionally, because of the pipetting method, isolated single cells showed large variations in their relative positioning within the rectangular microwells which leads to a bias when sensing in a temporal manner. When compared, we report two times greater single T cell per microwell efficiency (**Table 1**). The improved efficiency is reasoned to the associated pressure oscillations with the airplugs at the air–liquid interface. In the literature, airplugs are generally utilized in several biological applications such as cell patterning,[40] rotational cell manipulation,[41] and formation of blood droplets.[42]

The presented device can be scaled up by increasing the number of loading channels and microwells for higher throughput. Additionally, advanced localized cell entrapment can be achieved by either selectively shifting the typical "straight" cell loading channel with respect to the center of the microwells or with its angular misalignment relative to the microwells' central axis. Also,

Table 1. Comparison of the developed device in this study with a similar reported device[22] for the isolation of single T cells in rectangular microwells.

Model cell line	Number of microwells	Microwell volume [nL]	Sedimentation time [h]	Single cell isolation [%]	Reference
Jurkat	2250	0.50	0.5	19.7	This study
U937	5440	0.54	24	8.7	[22]

the cell loading channel can be designed with different shapes such as zigzag or wave-like. Finally, different rows of microwells can be functionalized with different antibodies for selective central entrapment/capture of different sub-types of T immune cells (e.g., $CD4^+$ T cell and $CD8^+$ T cell) and/or other immune cells such as B and NK (Natural killer) cells. Here, by using optimized parameters (e.g., flow rate, sedimentation time, antibody concentration) and blocking non-specific binding sites on the microwells, it is expected that the single cell occupancy per microwell would be the same (about 20%). Nonetheless, in the future, isolation of immune cells from highly inhomogeneous population of cells (like blood cells) can help elucidate precisely the immune response of cells at single cell level, especially for phenotyping and biotherapeutics studies.

4. Experimental Section

Device Fabrication and Alignment: The design of the cell loading and microwell layers were carried out using AutoCAD software. A chrome photomask (10 µm resolution) was obtained from Front Range PhotoMask, LLC, USA. The microchannels and microwells were fabricated in-house using SU-8 negative photoresist (MicroChem Corp., USA). Briefly, SU-8 was spin-coated on a 4-inch diameter silicon wafer at 100 rpm and at 3700 rpm for 5 s each, which formed a 20 µm thick photoresist. Then, the photoresist was soft-baked on hot plate at 65 °C for 1 min and at 95 °C for 5 min. Following, the photoresist was printed using MA8 mask aligner (SUSS MicroTech SE, Germany) and exposed to UV light at a power of 10 mW cm^{-2} and an exposure dose of 240 mJ cm^{-2} for 36 s each. After its baking on hot plate at 65 °C for 1 min and at 95 °C for 3 min, the photoresist was developed using SU-8 developer and washed using isopropyl alcohol (IPA) and deionized (DI) water for 60 s. Then, PDMS-based Sylgard 184 elastomer (Dow Corning Corp., USA) and a curing agent were mixed at a 10:1 w/w ratio, poured onto the master cell loading and microwell molds, and degassed and cured in oven at 60 °C for 3 h. The cured PDMS molds were then peeled off, and after puncturing the inlets and outlets of channels, the cell loading and microwell layers were aligned under the microscope to form the device. Finally, the device was placed in oven to anneal at 60 °C for overnight.

Airplug Formation and Release: Platinum-cured silicone tubings (1/32" ID × 3/32" OD) were used to connect the syringes to the PDMS device. Then, phosphate buffered saline (PBS; SigmaAldrich) was passed at 500 µL h^{-1} flow rates through the channels using neMESYS syringe pump (Cetoni GmbH, Germany) in order to generate airplugs within the microwells. Once the PBS reached the outlet of the channels, the flow was stopped and generated airplugs were used to isolate single cells in between airplugs of the microwells. The release of the airplugs was carried out at 200 µL h^{-1} flow rate using PBS.

Cell Culture: $CD3^+$ T cells (human lymphocyte Jurkat T cell line) were purchased from American Type Culture Collection (ATCC) and suspended in Roswell Park Memorial Institute (RPMI; Sigma-Aldrich) medium supplemented with 10% fetal bovine serum (FBS; Sigma-Aldrich) and 1% penicillin-streptomycin (Pen-Strep; Sigma-Aldrich). Then, cells were incubated in a humidifying incubator at 37 °C and 5% CO_2. When about 80% confluent, cells were passaged and used in the single cell isolation and centralization experiments. For counting, cells were stained with green CellTracker (FisherScientific) for 15 min at room temperature in dark. Then, cells were centrifuged and washed twice and loaded to syringes at 10^6 cells mL^{-1} concentrations.

Single T Cell Isolation in Microwells: To isolate T cells, 25 µL of the cell suspension was passed through the PDMS device at 100 µL h^{-1} flow rate and five sequential pulsatile flows were applied using 5 µL cell suspension. After each pulsation, cells were allowed to sediment in the microwells for 5 min. Then, PBS was passed at 200 µL h^{-1} to release the airplugs.

Centralization of T Cells: The ani-$CD3^+$ antibodies were used to selectively capture and centralize T cells in microwells through antibody–antigen interactions. The antibody immobilization was carried out on microwell surfaces confined by airplugs using the linker protocol described previously.[34] Briefly, 5 µL of PBS solution containing 2% v/v 3-aminopropyltriethoxysilane (APTES; SigmaAldrich) was first passed through the PDMS device at 20 µL h^{-1} flow rate and allowed to silanize the microwells for 60 min at room temperature. Then, the heterobifunctional cross-linker, *N*-[ß-maleimidopropyloxy]-succinimide ester (BMPS; SigmaAldrich), was dissolved in PBS (3 mg mL^{-1}) and 5 µL of the solution was passed at 20 µg mL^{-1} flow rate and incubated for 60 min at room temperature to create maleimido-activated microwells. Following, a stock solution of purified antihuman $CD3^+$ antibodies (BioLegend) was diluted in sterile PBS to 20 µg mL^{-1} concentrations and 7 µL antibody aliquot was passed at 20 µL h^{-1} flow rate and incubated for 60 min at room temperature to coat the microwells with antibodies. T cells were then loaded following the steps described in the single T cell isolation section. PBS was then passed at 200 µL h^{-1} to release the airplugs and the cell loading layer was peeled off from microwell layer to evaluate the displacement of the cell relative to their initial position in the microwells. In brief, within the microwells, positive cell displacement indicated the one above cells' original location, whereas negative cell displacement indicated the one below cells' original location. In both cases, cells were regarded as decentralized cells (Figure S1b, Supporting Information).

Cytokine Release and Detection: 100 ng mL^{-1} of PMA and 1000 ng mL^{-1} of ionomycin were dissolved in DI water in 1:1 v/v ratio and the solution was added to the T cell suspension of $\approx 10^6$ cells mL^{-1} in PBS. The cells were then loaded into microwells. Immediately after, the anti-IL-2 antibodies (MAB602, R&D Systems; covalently immobilized as stripes on the glass slides using APTES-BMPS chemistry) were placed on the top of the microwells and the cytokine release was allowed for 60, 120, and 240 min of incubation. Afterward, secondary anti-IL-2 antibodies (AF-202-NA, R&D Systems; conjugated to red Alexa Fluor 594 dyes and used at 20 µg mL^{-1} concentration) were used to measure the IL-2 release from the single T cells. As a final step, the viability of cells was confirmed using calcein AM (green fluorescent dye, live cells) and ethidium homodimer-1 (red fluorescent dye, dead cells).

Microscopy Imaging: Bright field and fluorescent (using green fluorescein isothiocyanate, FITC, or red Texas Red filter cubes) images were acquired with Nikon Ti Eclipse inverted microscope and through 4× objective lens with 0.20 numerical aperture. Characterization of isolated and localized cells was carried out using ImageJ software.

Numerical Modeling: The finite element analysis software, COMSOL Multiphysics, was used in modeling, where two cytokine release scenarios were considered: 1) continuous release of IL-6 and 2) 10-s release of IL-6. These were implemented in the model by representing the cell as a time dependent source of IL-6. All other boundaries were taken as solid walls. Diffusion coefficient of IL-6 was set as 2.7×10^{-7} cm^2 s^{-1} and the surrounding fluid was modeled as water.[43]

Analytical Solution: Numerical model was confirmed by analytically solving the following 2D diffusion equation:

$$D_x \frac{\partial^2 c}{\partial x^2} + D_y \frac{\partial^2 c}{\partial y^2} = \frac{\partial c}{\partial t} \quad (1)$$

And considering an unbounded 2D domain with the following initial conditions:

$$C\,(x = 0, y = 0, t = 0) = M\partial\,(x, y) \quad (2)$$

Where ∂ is the Kronecker delta, and

$$\partial\,(x, y) = 0 for x, y \neq 0 \text{ and } \partial\,(x) = 1 \text{ for } x, y = 0 \quad (3)$$

Together with the boundary conditions:

$$\text{When } x \to \infty;\ \frac{\partial c}{\partial x},\ C \to 0 \quad (4)$$

$$\text{When } y \to \infty;\ \frac{\partial c}{\partial y},\ C \to 0 \quad (5)$$

The solution to these equations gives the transient concentration gradient within the domain and can be solved using the separation of variables method to give

$$C\,(x, y, t) = A_{(t)} e^{-\left(\frac{x^2}{4D_x t} + \frac{y^2}{4D_y t}\right)} \quad (6)$$

Where $A_{(t)}$ is the magnitude of concentration at when $x, y = 0$(surface of the cell) and for a relative reference value of 1:

$$C\,(x, y, t) = e^{-\left(\frac{x^2}{4D_x t} + \frac{y^2}{4D_y t}\right)} \quad (7)$$

To minimize the complexity in deriving an exact analytical solution, the microchannels were modelled as infinitely long domains. However, since numerical modeling of an infinitely long domain is unfeasible, the channels were modelled on COMSOL as 400 μm long domains with all other boundary conditions remaining the same.

Statistical Analysis: All experiments were performed in triplicates ($n = 3$) and data was presented as mean ± SD or mean ± SEM. Statistical analysis was performed with Origin software (OriginLab Corp., USA) using *t*-test analysis. A p-value < 0.05 was considered statistically significant.

Supporting Information

Supporting Information is available from the Wiley Online Library or from the author.

Acknowledgements

This research was financially supported by NYU Global Seed Grant for Collaborative Research, as well as by National Science Foundation (CBET 1701322) and by National Institutes of Health (1R21EB025406 and R35GM133646). The authors acknowledge Mr. Ayoub Gila for designing the microfluidic sensing stripes, and the Core Technology Platforms at New York University Abu Dhabi (NYUAD) for use of its clean room facilities. A.T.B. acknowledges NYUAD Global Ph.D. Fellowship.

Conflict of Interest

The authors declare no conflict of interest.

Keywords

airplugs, centralization, microfluidics, microwells, T cells

Received: May 29, 2019
Revised: September 23, 2019
Published online:

[1] B. Walker, A. McMichael, *Cold Spring Harb. Perspect. Med.* **2012**, *2*, a007054.
[2] S. B. Bradfute, K. L. Warfield, S. Bavari, *J. Immunol.* **2008**, *180*, 4058.
[3] M. A. Reuter, C. Pombo, M. R. Betts, *Cytokine Growth Factor Rev.* **2012**, *23*, 181.
[4] C. Ma, R. Fan, H. Ahmad, Q. Shi, B. Comin-Anduix, T. Chodon, R. C. Koya, C. C. Liu, G. A. Kwong, C. G. Radu, A. Ribas, J. R. Heath, *Nat. Med.* **2011**, *17*, 738.
[5] S. J. Lo, D. J. Yao, *Int. J. Mol. Sci.* **2015**, *16*, 16763.
[6] D. K. Mishra, H. J. Rocha, R. Miller, M. P. Kim, *Sci. Rep.* **2018**, *8*, 8.
[7] S. Yilmaz, A. K. Singh, *Curr. Opin. Biotechnol.* **2012**, *23*, 437.
[8] T. M. Gierahn, M. H. Wadsworth, T. K. Hughes, B. D. Bryson, A. Butler, R. Satija, S. Fortune, J. C. Love, A. K. Shalek, *Nat. Methods* **2017**, *14*, 395.
[9] Y. Deng, Y. Zhang, S. Sun, Z. Wang, M. Wang, B. Yu, D. M. Czajkowsky, B. Liu, Y. Li, W. Wei, Q. Shi, *Sci. Rep.* **2014**, *4*, 7499.
[10] H. E. Karakas, J. Kim, J. Park, J. M. Oh, Y. Choi, D. Gozuacik, Y. K. Cho, *Sci. Rep.* **2017**, *7*, 2050.
[11] S. S. Bithi, S. A. Vanapalli, *Sci. Rep.* **2017**, *7*, 41707.
[12] X. L. He, F. Lu, F. L. Yuan, D. L. Jiang, P. Zhao, J. Zhu, H. L. Chene, J. Cao, G. Z. Lu, *Antimicrob. Agents Chemother.* **2015**, *59*, 4817.
[13] S. H. Kim, T. Fujii, *Lab Chip* **2016**, *16*, 2440.
[14] Y. Chen, S. Li, Y. Gu, P. Li, X. Ding, L. Wang, J. P. McCoy, S. J. Levine, T. J. Huang, *Lab Chip* **2014**, *14*, 924.
[15] C. Sun, H. Hassanisaber, R. Yu, S. Ma, S. S. Verbridge, C. Lu, *Sci. Rep.* **2016**, 6, 29407.
[16] Y. C. Chen, S. G. Allen, P. N. Ingram, R. Buckanovich, S. D. Merajver, E. Yoon, *Sci. Rep.* **2015**, *5*, 9980.
[17] S. M. Kim, S. H. Lee, K. Y. Suh, *Lab Chip* **2008**, *8*, 1015.
[18] M. Hosokawa, A. Arakaki, M. Takahashi, T. Mori, H. Takeyama, T. Matsunaga, *Anal. Chem.* **2009**, *81*, 5308.
[19] K. Zhang, M. Gao, Z. Chong, Y. Li, X. Han, R. Chen, L. Qin, *Lab Chip* **2016**, *16*, 4742.
[20] J. Chung, Y. J. Kim, E. Yoon, *Appl. Phys. Lett.* **2011**, *98*, 123701.
[21] B. R. Oh, P. Chen, R. Nidetz, W. McHugh, J. Fu, T. P. Shanley, T. T. Cornell, K. Kurabayashi, *ACS Sens.* **2016**, *1*, 941.
[22] Y. Lu, J. J. Chen, L. Mu, Q. Xue, Y. Wu, P. H. Wu, J. Li, A. O. Vortmeyer, K. Miller-Jensen, D. Wirtz, R. Fan, *Anal. Chem.* **2013**, *85*, 2548.
[23] Y. Lu, Q. Xue, M. R. Eisele, E. S. Sulistijo, K. Brower, L. Han, E. D. Amir, D. Pe'er, K. Miller-Jensen, R. Fan, *Proc. Natl. Acad. Sci. U. S. A.* **2015**, *112*, E607.
[24] J. Y. Zhu, J. C. He, M. Verano, A. T. Brimmo, A. Glia, M. A. Qasaimeh, P. Y. Chen, J. O. Aleman, W. Q. Chen, *Lab Chip* **2018**, *18*, 3550.
[25] P. Y. Chen, M. T. Chung, W. McHugh, R. Nidetz, Y. W. Li, J. P. Fu, T. T. Cornell, T. P. Shanley, K. Kurabayashi, *ACS Nano* **2015**, *9*, 4173.
[26] Q. Han, N. Bagheri, E. M. Bradshaw, D. A. Hafler, D. A. Lauffenburger, J. C. Love, *Proc. Natl. Acad. Sci. U. S. A.* **2012**, *109*, 1607.
[27] H. Zhu, G. Stybayeva, J. Silangcruz, J. Yan, E. Ramanculov, S. Dandekar, M. D. George, A. Revzin, *Anal. Chem.* **2009**, *81*, 8150.
[28] X. K. Li, M. Soler, C. Szydzik, K. Khoshmanesh, J. Schmidt, G. Coukos, A. Mitchell, H. Altug, *Small* **2018**, *14*, 1800698.
[29] Q. Han, E. M. Bradshaw, B. Nilsson, D. A. Hafler, J. C. Love, *Lab Chip* **2010**, *10*, 1391.
[30] E. Choy, S. Rose-John, *JSRD* **2017**, *2*, S1.
[31] S. Shin, J. Seo, H. Han, S. Kang, H. Kim, T. Lee, *Materials* **2016**, *15*, 9.

[32] B. D. Liu, B. H. Tian, X. Yang, M. Li, J. H. Yang, D. S. Li, K. W. Oh, *Biomicrofluidics*, **2018**, *12*, 034111.
[33] F. Shen, X. J. Li, P. C. H. Li, *Biomicrofluidics* **2014**, *8*, 014109.
[34] M. Deliorman, M. L. Wolfenden, Z. Suo, I. B. Beech, X. Yang, R. Avci, in *Understanding Biocorrosion: Fundamentals and Applications* (Eds: T. Liengen, R. Basseguy, D. Feron, I. B. Beech), Woodhead Publishing, Cambridge, UK, **2014**, Ch. 6, pp. 145–165.
[35] F. Z. El Hentati, F. Gruy, C. Iobagiu, C. Lambert, *Cytometry, Part B* **2010**, *78b*, 105.
[36] A. Valle, G. Barbagiovanni, T. Jofra, A. Stabilini, L. Perol, A. Baeyens, S. Anand, N. Cagnard, N. Gagliani, E. Piaggio, M. Battaglia, *J. Immunol.* **2015**, *194*, 2117.
[37] C. Pasare, R. Medzhitov, *Nature* **2005**, *438*, 364.
[38] J. A. Ledbetter, L. E. Gentry, C. H. June, P. S. Rabinovitch, A. F. Purchio, *Mol. Cell. Biol.* **1987**, *7*, 650.
[39] S. H. Chiu, C. H. Liu, *Lab Chip*, **2009**, *9*, 1524.
[40] V. N. Goral, S. H. Au, R. A. Faris, P. K. Yuen, *Lab Chip* **2015**, *15*, 1032.
[41] D. Ahmed, A. Ozcelik, N. Bojanala, N. Nama, A. Upadhyay, Y. Chen, W. Hanna-Rose, T. J. Huang, *Nat. Commun.* **2016**, *7*, 11085.
[42] X. Huang, W. Hui, C. Hao, W. Yue, M. Yang, Y. Cui, Z. Wang, *Small* **2014**, *10*, 758.
[43] G. J. Goodhill, *Eur. J. Neurosci.* **1997**, *9*, 1414.

Supporting Information

Airplug-mediated isolation and centralization of single T cells in rectangular microwells

*Pavithra Sukumar, Muhammedin Deliorman, Ayoola T. Brimmo, Roaa Alnemari, Deena Elsori, Weiqiang Chen, and Mohammad A. Qasaimeh**

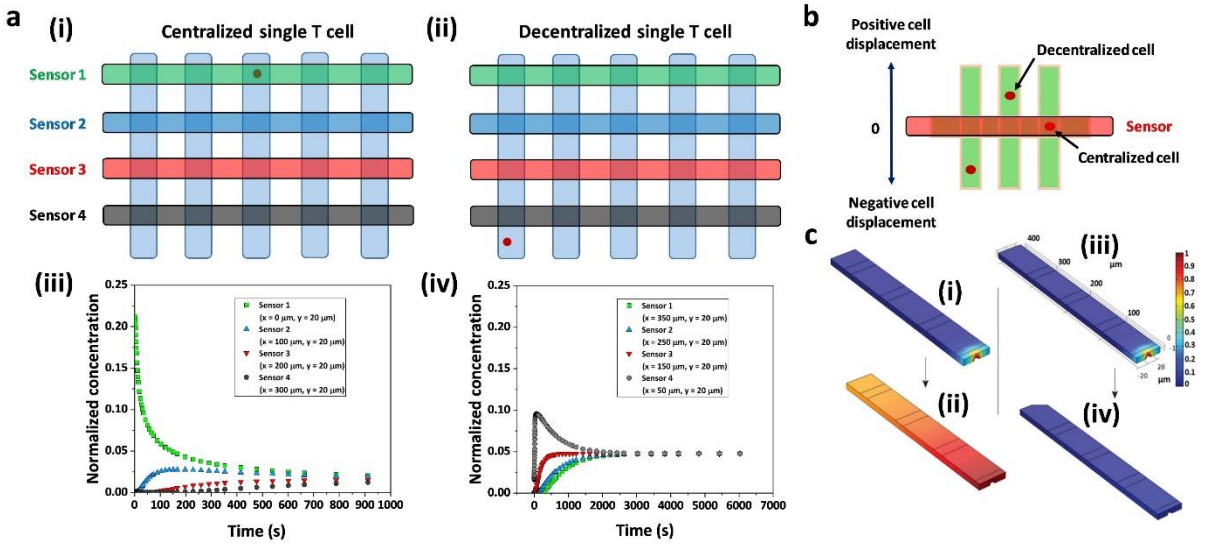

Figure S1. Bias in cytokine sensing. (a) Schematics representing the positioning of single T cells (red dots) with respect to the sensors when they are (i) centralized and (ii) decentralized. Graphs show the instantaneous releases of interleukin-6 (IL-6) proteins from a centralized (iii) and decentralized (iv) T cell as detected by sensors 1-4 positioned 100 µm apart from each other. (b) Illustrative schematic shows the relative change in cells' positions within the microwells relative to their initial (i.e. centralized) positions relative to the sensor, where decentralized cells show displacements towards positive or negative sides of the microwells along the cell loading channel. (c) Concentration gradient of IL-6 at: (i) 10 seconds and (ii) 3000 seconds after initial IL-6 release in a model where IL-6 was assumed to be released by the cell continuously; and (iii) 10 seconds and (iv) 500 seconds after initial release IL-6 release in a model where IL-6 was assumed to be released by the cell for only 10 seconds.

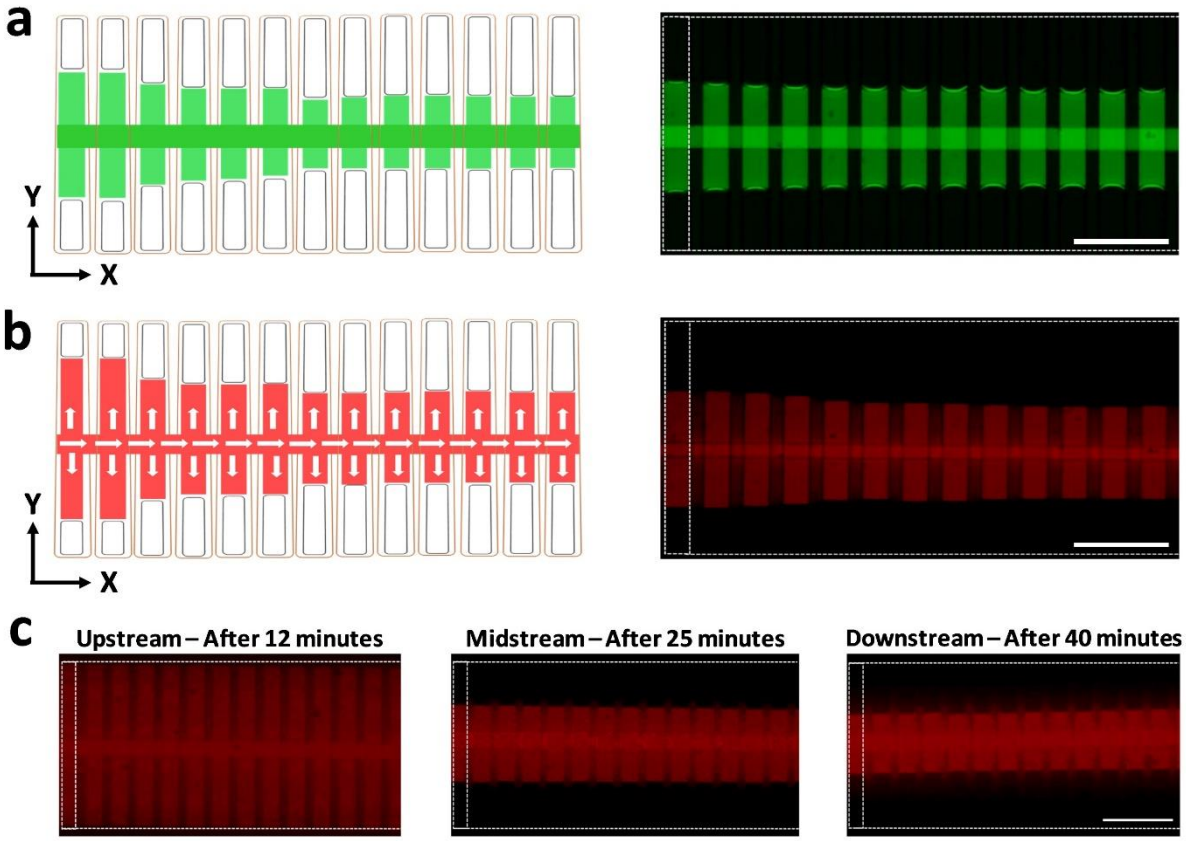

Figure S2. Characterization of airplug release. (a) Illustrative schematics and fluorescence images show the formed airplugs within the microwells following passing fluorescein dyes (green) at 500 µL/h flow rate. (b) Rhodamine dyes (red) were used to visualize the airplug release dynamics from the microwells when they were passed at 200 µL/h flow rate. The white arrows indicate the direction of the extension of rhodamine dyes during the airplug compression/release. (c) Further fluorescence images taken during the pass of rhodamine dyes at 200 µL/h flow rate revealed that the release of the airplugs in the upstream sections after 12 minutes was faster as compared to the release of the airplugs in the midstream (after 25 minutes) and downstream (after 40 minutes) sections. Scale bars in (a-c) are 200 µm.

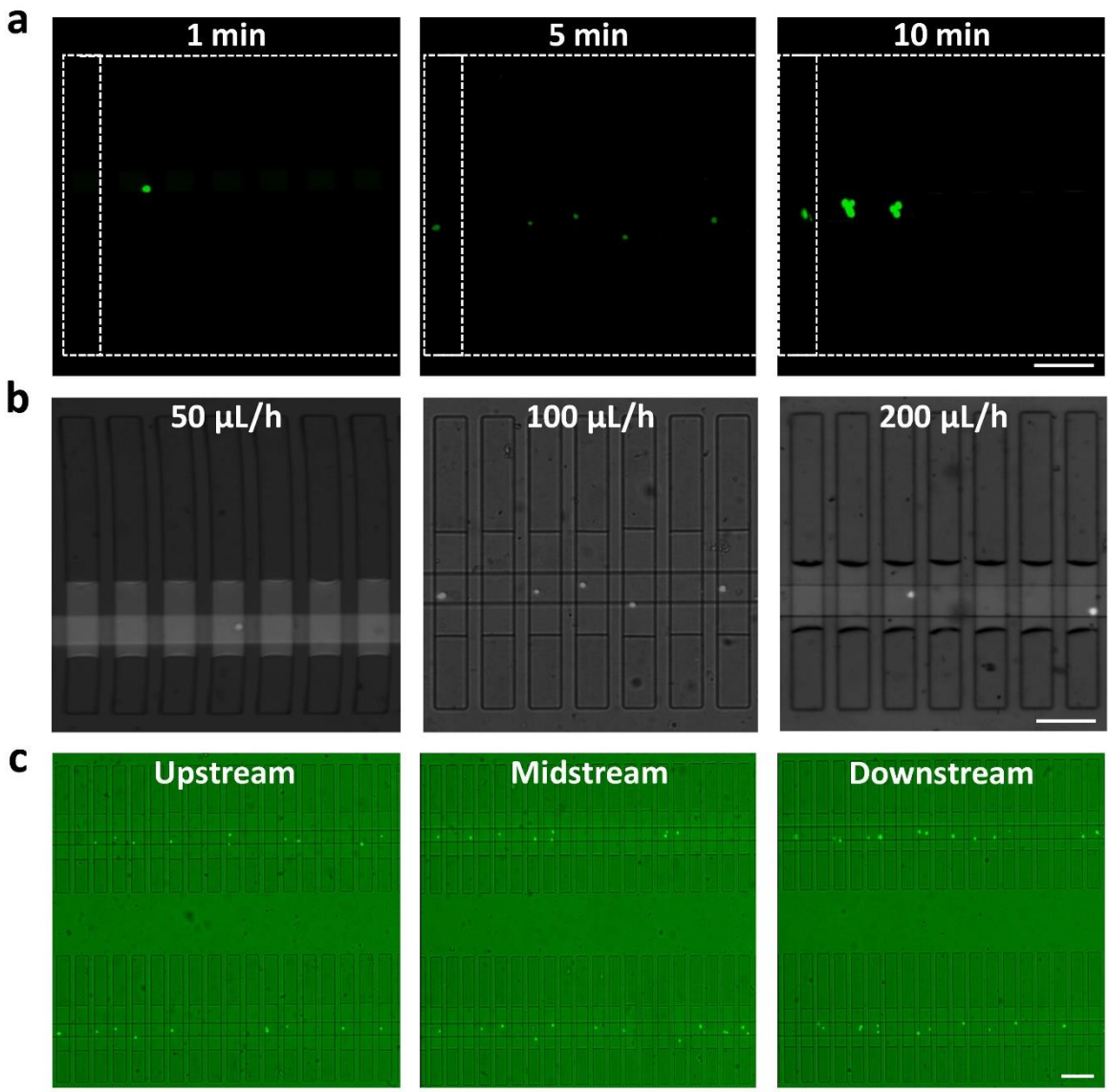

Figure S3. Airplug-mediated single sell isolation. (a) Representative fluorescent images show cells isolated through 1-, 5-, and 10-minute sedimentation times following 100 µL/h pulsatile flow rates and five pulses. (b) Representative bright field microscopy images show single cells isolated at 5-minute sedimentation time following 50, 100, and 200 µL/h pulsatile flow rates and five pulses. (c) Representative fluorescence images show cells isolated at upstream, midstream, and downstream sections of the microfluidic channel. Scale bars in (a-c) are 150 µm.

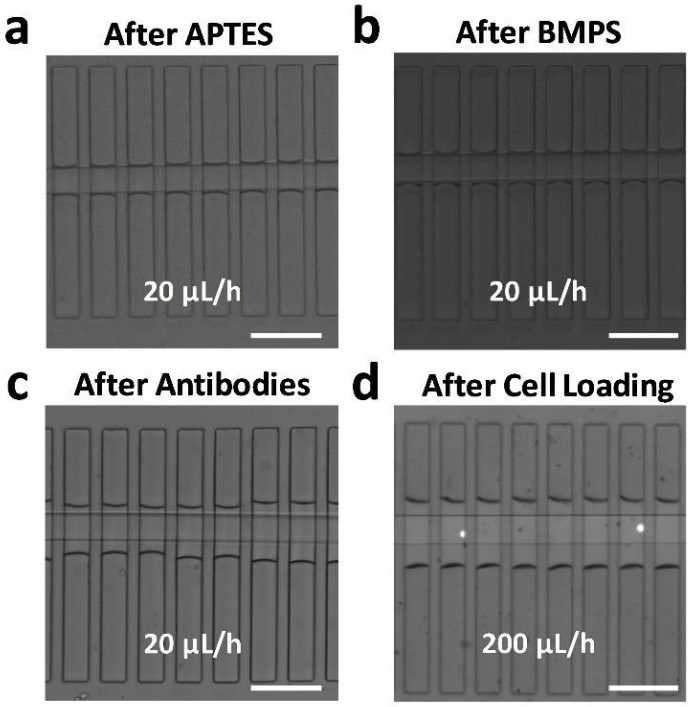

Figure S4. Variation of airplug lengths during antibody immobilization steps. (a-c) Bright field microscopy images show that passing solutions of APTES, BMPS, and antibodies at 20 µL/h flow rates did not significantly change the length of the airplugs within the microwells. (d) A bright field microscopy image shows centralized cells (bright dots) during the airplug release at 200 µL/h flow rate using PBS. Scale bars in (a-d) are 200 µm.

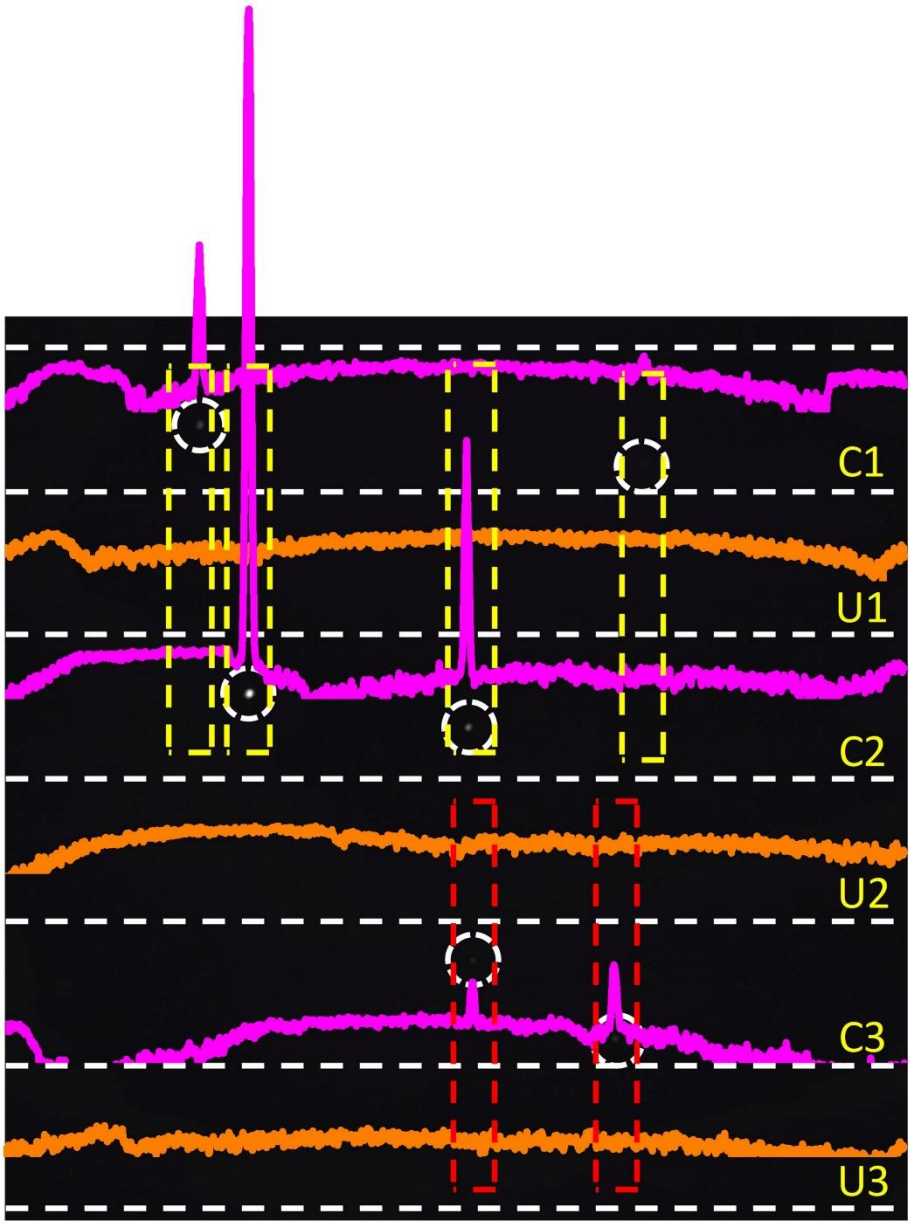

Figure S5. Bias in sensing. Fluorescence image shows the detected IL-2 spots (white-dashed circles) following stimulation of the T cells for 240 minutes with PMA/ionomycin within the microwells of the device. The location of each of the antibody sensing stripes (C1, C2, and C3) and the uncoated regions (U1, U2, and U3) in between them are also shown for clarity. These regions (each 100 μm in width) where designed in a way that three of them can fit the microwells in the device (e.g., C1-U1-C2 and U2-C3-U3 for the yellow- and red-dashed rectangles, respectively). Clearly, the differences in the spot intensity of the released IL-2 reveals the heterogeneity among the stimulated single cells. The bias in sensing due to position of cells relative to sensing stripes is also achieved, although visualizing this bias experimentally would require an imaging where noise-to-signal ratio is low in the background. Additionally, our simulation results suggested that the C1 stripe would sense in C2 the cytokines released from the cells positioned in yellow-dashed rectangles within 40 minutes of its secretion (or vice versa). In the experimental data, however, seemingly more time would be needed for the bias to be visually detectable.